

An ASCA-ROSAT Study of the Distant, Lensing Cluster A2390

H. Böhringer¹, Y. Tanaka^{1,2}, R.F. Mushotzky³, Y. Ikebe¹, M. Hattori⁴,

¹ Max-Planck-Institut für Extraterrestrische Physik, D-85748 Garching, Germany

² Institute of Space and Astronautical Science, Sagami-hara, Kanagawa 229, Japan,

³ Laboratory for High Energy Astrophysics, Code 660, NASA/Goddard Space Flight Center, Greenbelt, MD 20771, USA

⁴ Astronomical Institute, Tohoku University, Aoba Aramaki, Sendai, Japan

Received ; accepted

Abstract. We present the results of a combined study of ASCA and ROSAT observations of the distant cluster Abell 2390. For this cluster a gravitational arc as well as weak lensing shear have been previously discovered.

We determine the surface brightness profile and the gas density distribution of the cluster from the ROSAT PSPC and HRI data. A combined spatially resolved spectral analysis of the ASCA and ROSAT data show that the temperature distribution of the intracluster medium of A2390 is consistent with an isothermal temperature distribution in the range 9 to 12 keV except for the central region. Within a radius of $160h_{50}^{-1}$ kpc the cooling time is found to be shorter than the Hubble time, implying the presence of a cooling flow. In this central region we find strong evidence for a multi-temperature structure. Detailed analysis of the combined ASCA and ROSAT data yields a self-consistent result for the spectral structure and the surface brightness profile of the cluster with a cooling flow of about $500 - 700 M_{\odot} y^{-1}$ and an age of about 10^{10} y.

From the constraints on the temperature and density profile of the intracluster gas we determine the gravitational mass profile of the cluster and find a mass of about $2 \cdot 10^{15} M_{\odot}$ within a radius of $3h_{50}^{-1}$ Mpc. A comparison of the projected mass profiles of the cluster shows an excellent agreement between the mass determined from X-ray data and the mass determined from the models for the gravitational arc and the weak lensing results. This agreement in this object, as compared to other cases where a larger lensing mass was implied, may probably be due to the fact that A2390 is more relaxed than most other cases for which gravitational lensing mass and X-ray mass have been compared so far.

Key words: dark matter - gravitational lensing - Galaxies: clusters: individual: A2390 - cooling flows - Xrays: galaxies

1. Introduction

A 2390 is one of the most prominent clusters in the redshift range around $z = 0.2$. It was classified by Abell (1958) and Abell, Corwin & Olowin (1989) only as a richness class 1 cluster. As a target of the CNOC survey (Yee et al. 1996a) deep photometric and spectroscopic data were obtained for this cluster, and these authors conclude that it should more likely be classified as a richness class 3 cluster (Yee et al. 1996b). This new CNOC data also provide a mean redshift for this cluster of $z=0.228$ (compared to the previous literature value of $z=0.232$ by Le Borgne et al. 1991).

In X-rays it is among the ten brightest galaxy clusters known at a redshift larger than 0.18 (e.g. Ebeling et al. 1996). It has been observed with the EINSTEIN observatory and showed a luminosity of $L_x \sim 1.6 \cdot 10^{45}$ erg s^{-1} (in the 0.7 to 3.5 keV energy band) (Ulmer et al. 1986; if their result is converted to $H_0 = 50$ km s^{-1} Mpc $^{-1}$ as used in this paper) and the cluster has a slightly elongated shape (McMillian et al. 1989). A “straight arc” and several arclets were discovered in this clusters by Pello et al. (1991). All these observations underline that A2390 is a very rich and massive cluster of galaxies.

Pierre et al. (1996) have analyzed a deep ROSAT HRI observation and found that the X-ray emission from A2390 is very concentrated and highly peaked, indicating a strong cooling flow of about $880 M_{\odot} y^{-1}$. The cooling flow is centered on the giant elliptical galaxy in the cluster center. This together with the observation of the strong lensing features may indicate that the very peaked central surface brightness is probably the effect of the cooling flow as well as of a steep central gravitational potential in the cluster.

The straight arc has been modeled by Kassiola, Kovner, & Blandford (1992) and Narashima & Chitre (1993). Pierre et al. (1996) have also modeled the lensing cluster with an elliptical potential model and a second clump in close consistency with the X-ray morphology. They find a projected mass within the arc radius of

$M(r \leq 38'') \sim 0.8 \cdot 10^{14} h^{-1} M_{\odot}$. They compared the lensing mass with the X-ray data by taking the mass profile of the lensing model and the gas density profile from the X-ray surface brightness, and calculated the temperature profile needed to satisfy the hydrostatic equation. The bulk temperatures found by this approach are in the range 8 to 10 keV. This high temperature is consistent with the large X-ray luminosity of the cluster given the generally good correlation between X-ray ICM temperature and X-ray luminosity (e.g. Edge & Stewart 1991).

A weak lensing shear in A2390 was also observed recently by Squires et al. (1996). They deduced an elliptical mass distribution, elongated in the direction of the straight arc. This is qualitatively consistent with the X-ray surface brightness distribution. As we will show in this paper the mass distribution inferred from the X-ray results are in excellent agreement with both the mass deduced from the weak lensing analysis and that from the strong lensing modeling.

The detection of diffuse intracluster light was reported by Vílchez-Gómez et al. (1994). This may also be taken as a sign that the core of the cluster is relaxed and that the debris of tidal stripping of galactic halo material had enough time to settle in the gravitational potential of the cluster.

All these previous studies and the fact that the cluster is very massive and X-ray luminous makes A2390 a perfect target for more detailed X-ray observations, in particular to compare a more precise mass determination from the X-ray data with the optical and lensing results. The indication of the fair agreement of the mass in the different previous studies and the existence of the strong cooling flow suggest that the cluster is essentially relaxed and therefore ideal for the test of the various methods of mass determination.

In this paper we present a combined analysis of deep ASCA and ROSAT PSPC and HRI observations of this cluster. The ROSAT observations are discussed in Section 2 and the ASCA observations in Section 3. A combined analysis of the spectral data of both instruments which provides very interesting evidence for multi-temperature structure in the cooling flow region of A2390 is presented in Section 4. Section 5 contains the results of the cluster mass determination from the X-ray data, and compared to the lensing results in Section 6. The cooling flow structure is discussed in detail in Section 7. Section 8 provides a summary and conclusions. We use a value of $H_0 = 50 \text{ km s}^{-1} \text{ Mpc}^{-1}$ for the Hubble constant throughout this paper. Thus 1 arcmin at the distance of A2390 corresponds to a scale of $277 h_{50}^{-1} \text{ kpc}$.

2. ROSAT Observations

A2390 was observed with the ROSAT PSPC in November 1993 for 10336 sec. About 5100 source photons were registered in the ROSAT hard band (channels 52 to 201)

corresponding to the energy range 0.5 to 2.0 keV. The X-ray emission could be traced out significantly to a maximum radius of 9 arcmin ($2.5 h_{50}^{-1} \text{ Mpc}$). There are a few point sources inside the 9 arcmin radius and more point sources surrounding the cluster. Taking the brightest five of the inner point sources we find that they contribute only about 2% to the X-ray flux of the cluster in the PSPC hard band. We therefore conclude that the contamination by the point sources is negligible. The count rate within a 9 arcmin radius (without the 2% correction) of $0.49 \pm 0.01 \text{ s}^{-1}$ yields an X-ray flux in the 0.1 to 2.4 energy band of $1.2 \cdot 10^{-11} \text{ erg s}^{-1} \text{ cm}^{-2}$ and a cluster rest frame X-ray luminosity of $2.7 \cdot 10^{45} \text{ erg s}^{-1}$ (0.1 to 2.4 keV) for a hydrogen column density of $9 \cdot 10^{20} \text{ cm}^{-2}$ and a temperature of 9 keV (see below and Section 3 for the choice of these values). The bolometric luminosity calculated with these parameters is about $8 \cdot 10^{45} \text{ erg s}^{-1}$.

An X-ray image of the cluster produced from the PSPC hard band counts is shown in Fig. 1. The image has been smoothed by a variable Gaussian filter to show the cluster extent and some of the internal structure equally well. The maximum filter scale is $\sigma = 1$ arcmin. The image has been divided by the exposure map and corrected for vignetting and for the background contribution. The contour levels are logarithmically spaced. The X-ray surface brightness is strongly peaked toward the center, and the cluster image is elongated in the SE/NW direction as already observed by Pierre et al. (1996) in the HRI image. For the X-ray maximum of the PSPC image we find the J2000 coordinates, 21h 53m 37s and 17d 41m 41s, which coincide within 2" with the position of the central cD galaxy and the peak of the X-ray emission in the HRI image (Pierre et al. 1996).

We also produced an image from the HRI observation for comparison, which is shown in Fig. 2. Due to the lower detector sensitivity and higher background, the X-ray emission can only be traced to a smaller radius (about 3 - 4 arcmin) than in the PSPC image in spite of the larger exposure time of 27.7 ksec. The outermost contour in the HRI image corresponds roughly to the sixth contour level of the PSPC image. (Note that in Fig. 2, HRI image, the contours are linearly spaced). Interestingly, the cluster displays the largest degree of ellipticity at an intermediate radius between about 1 and 2.5 arcmin. Further out the cluster becomes more azimuthally symmetric.

The very peaked central surface brightness could either be a sign of a very strong cooling flow in the cluster, or it could in principle also result from a central point source. To exclude a strong influence of a point source we compare the surface brightness profile of the cluster in the HRI image with the point spread function (PSF) of the HRI. This is shown in Fig. 3, where one notes that the central surface brightness peak is not caused by a point source.

We have determined an azimuthally averaged surface brightness profile for the PSPC and HRI observation of

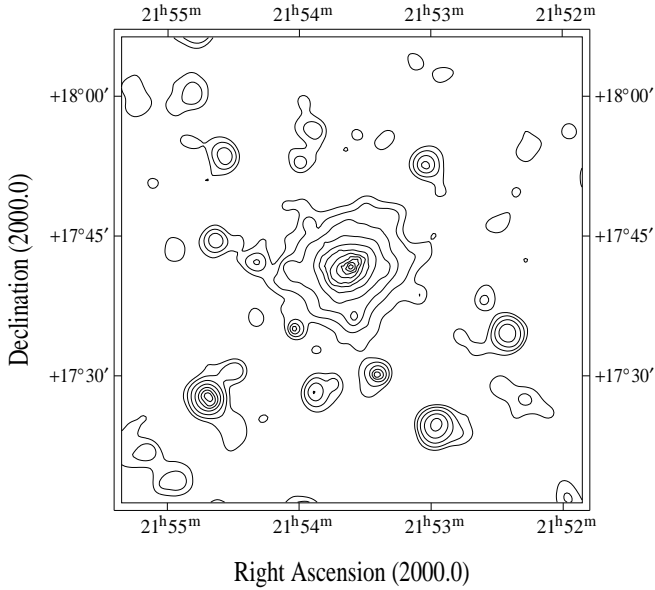


Fig. 1. ROSAT PSPC image of A2390 from a pointed observation with an exposure time of 10.3 ksec. The image is vignetting and background corrected, divided by the exposure map and smoothed with a variable Gaussian filter with a maximum width of $\sigma = 1$ arcmin. The contour levels start at a count rate surface brightness of $0.16 \text{ cts ksec}^{-1} \text{ arcmin}^{-2}$. The contours are logarithmically spaced and increase by factors of 2 (in linear scale).

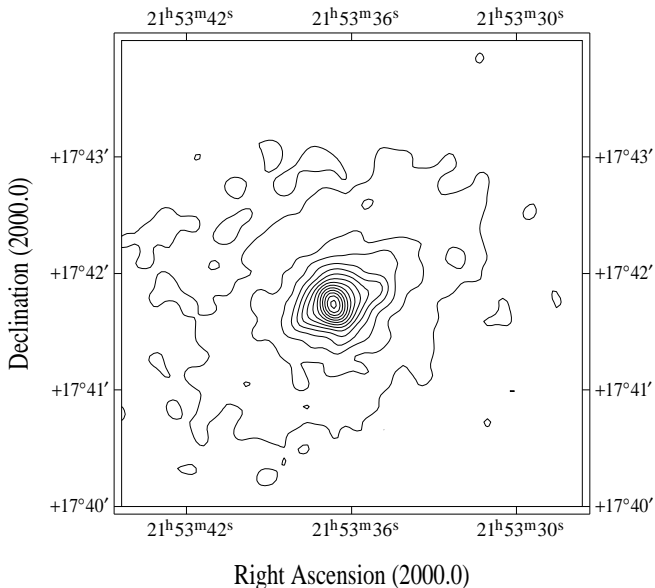


Fig. 2. Deep ROSAT HRI image of A2390 (see also Pierre et al. 1996). The image has been smoothed with a Gaussian filter with $\sigma = 4$ arcsec. For the background corrected image the first contour level corresponds to a count rate surface brightness of $9 \text{ cts ksec}^{-1} \text{ arcmin}^{-2}$ and the levels increase with steps of $13 \text{ cts ksec}^{-1} \text{ arcmin}^{-2}$.

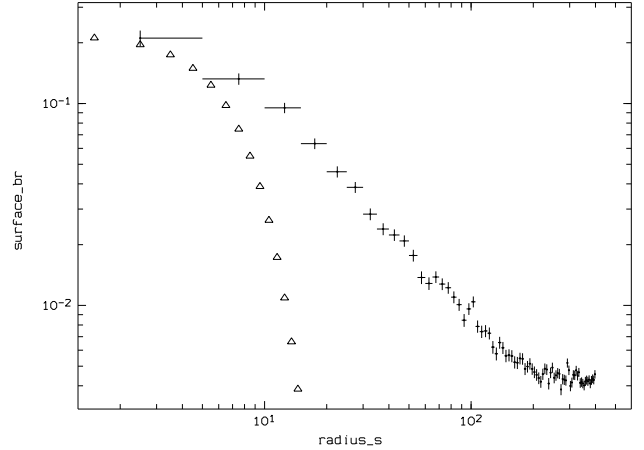


Fig. 3. Surface brightness profile of the central part of the ROSAT HRI image of A2390 (crosses). The surface brightness is given in units of $\text{cts s}^{-1} \text{ arcmin}^{-2}$ uncorrected for the background. The source surface brightness profile is compared to the profile of the point spread function of the HRI illustrating that the strongly, centrally peaked surface brightness profile is not due to the presence of a point source in the cluster.

Table 1. Results of the β -model fits to the surface brightness profiles of the ROSAT PSPC and HRI observations

data	S_0 $\text{cts s}^{-1} \text{ arcmin}^{-2}$	core radius arcsec	β	χ^2/ν
<i>HRI</i> ^{a)}	0.18	11.5	0.45	1.6
<i>PSPC</i> ^{a)}	0.18	35	0.62	1.8
<i>PSPC</i> ^{b)}	0.23	28	0.60	2.6

^a uncorrected for the HRI/PSPC PSF

^b corrected for the PSPC PSF

A2390. We fit a β -model (e.g. Cavaliere & Fusco-Femiano 1976, Jones & Forman, 1984) of the form

$$S(r) = S_0(r) \left(1 + \frac{r^2}{r_c^2} \right)^{-3\beta+1/2} \quad (1)$$

to both surface brightness profiles and found that the data can be described quite well by these analytical fits out to a radius of about 9 arcmin for the PSPC and about 3 arcmin for the HRI. The fitting results are summarized in Table 1. The PSPC surface brightness profile and the best fit model are shown in Fig. 4. We find a best fit core radius of 35 arcsec (close to the angular resolution of the PSPC). A comparison with the HRI profile, also shown in Fig. 4, reveals that the surface brightness keeps increasing in the inner part which is unresolved by the PSPC. However, the slope of the increase with decreasing radius is different in

the inner part. This is reflected in the different β values found in the PSPC and HRI data fits. The good overlap of the HRI and PSPC data at intermediate radii shows that the different slopes are not due to an inconsistency in the data.

In attempting to account for the central surface brightness excess we have also alternatively performed fits with composite profiles including a β -model and a Gaussian peak. We obtain a good fit with a significantly reduced χ^2 and $r_c = 47$ arcsec and $\beta = 0.66(\pm 0.04)$ which reflects the very slight steepening of the radial slope at larger radii (see below). This fitted profile deviates very little from the simple β -model at $r \geq 30$ arcsec, confirming the reliability of the simple β -model fit.

We have also fitted β -models convolved with the off-axis angle dependent point spread function (PSF) of the PSPC to the PSPC surface brightness data to determine the best fitting parameters for the real surface brightness profile. The result of these fits is also given in Table 1. For this PSF-corrected result a single β -model is no longer a good fit, since the break in the slope seen in the combined HRI/PSPC data is now also becoming evident in the PSPC profile. If the innermost points are skipped to determine the best fitting model for radii larger than ~ 30 arcsec, we find the same result as obtained from the PSPC data without taking into account the PSF. Therefore, we are using the latter result for the modelling of the cluster at larger radii.

Pierre et al. (1996) obtained the slope parameter β of 0.41 in their analysis of the HRI data. Their value indicates a slightly flatter central profile than our value. The difference is due to the fact that they restricted the fitting to the central 250 arcsec radius circle. The reason for this striking change of slope will become obvious below. We find that this change occurs at around 35 arcsec (~ 160 kpc), the cooling radius of the cluster ICM.

Bartelmann & Steinmetz (1996) claim that the β -model is not a good description of the X-ray surface brightness profile of clusters as found from their N-body-hydrodynamic simulations. They argue that the β -values determined in the fit depends critically on the background level and that this introduces a significant bias in the mass determination built on the β -model fits. We have carefully checked this problem for the present data. We find a best fit for the PSPC data of $\beta = 0.62$ with a formal error of ± 0.022 (90% confidence). If we perform separate fits to the inner and outer part of the surface brightness profile we find an indication of a slight steepening of the slope from $\beta = 0.56$ to $\beta = 0.66$. The corresponding difference in the resulting mass profile out to a radius of $3h_{50}^{-1}$ Mpc is less than 15% for the two extreme limits. Therefore, we can safely conclude that, within such an accuracy, the β -model fit to the surface brightness profile is a sufficiently good description for the cluster structure and mass analysis presented here.

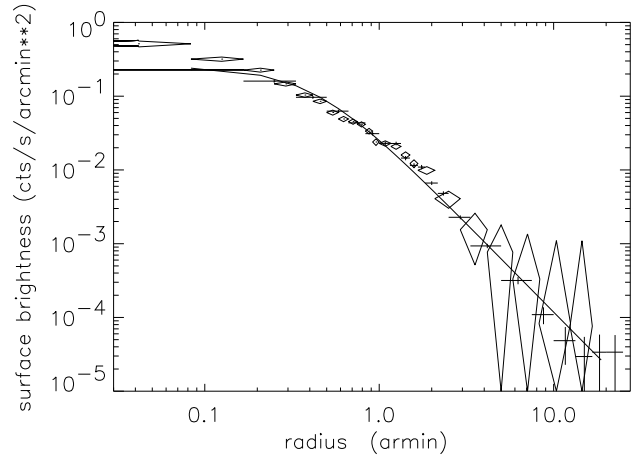


Fig. 4. X-ray surface brightness profile of A2390 determined from the ROSAT PSPC observation (crosses). The background is subtracted from the data taking into account a combined statistical and systematic error of 10% for the background determination. The fit of a β -model with the results given in Table 1 is shown by a solid line in this plot. The broadening of the profile due to the PSPC PSF is not taken into account in this fit. The surface brightness profile deduced from the HRI observation is overplotted (diamonds) for comparison. The HRI surface brightness in $\text{cts s}^{-1} \text{ arcmin}^{-2}$ was multiplied by a factor of 2.5 to account for the different detector sensitivity for the given spectral temperature and interstellar absorption.

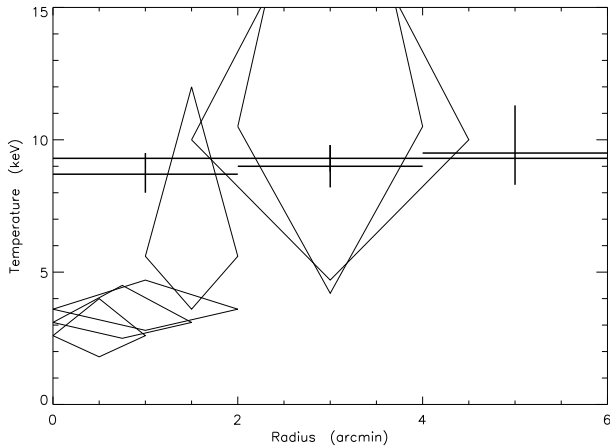
We analyze the PSPC spectra in concentric rings around the cluster center as defined by the position of the cD galaxy. The temperature for each annulus is determined by fitting the Raymond-Smith model. The result is summarized in Fig. 5. For the fits the element abundances were fixed to 0.3 of the solar values (see Section 3). The results clearly show a low temperature in the central region of the cluster inside about 2 arcmin ($kT \sim 3$ to 4 keV) as compared to the outer region. At larger radii the temperature is significantly higher, but due to the restricted low energy range of the ROSAT band the temperature cannot be well constrained. The hydrogen column density, N_H , determined within 2 arcmin radius is $(9.3 \pm 0.1) \cdot 10^{20} \text{ cm}^{-2}$, which is significantly higher than the hydrogen column density derived from 21cm surveys of $6.7 \cdot 10^{20} \text{ cm}^{-2}$ (Dickey & Lockman 1990; Stark et al. 1992). This discrepancy is discussed in Section 7.

3. ASCA Observation

A2390 was observed with ASCA on 20 June, 13 November, and 11 December, 1994, for a total exposure time of about 40 ksec. Both the GIS and SIS data are analysed. We subdivide the region within 6' from the center into three regions: the central circle of 2' radius and two annuli with radial ranges 2' - 4' and 4' - 6' from the center,

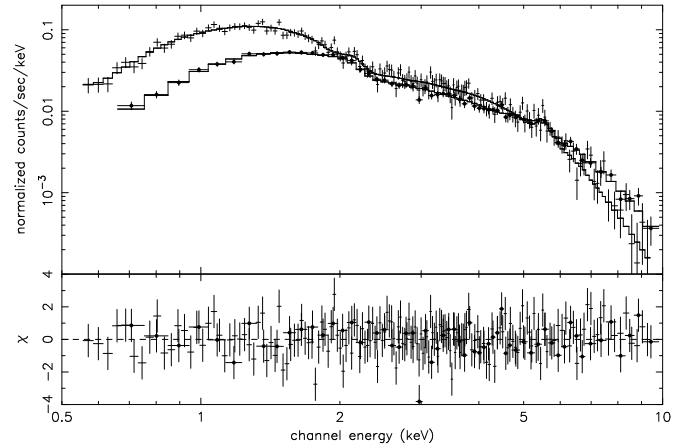
Table 2. Temperatures determined for concentric rings from the GIS data and from the combined GIS and SIS data

data	ring (arcmin)	kT (keV)	abundance ·solar	N_H (10^{21}cm^{-2})	χ^2/ν
GIS	0 – 2	8.6(7.6 – 9.8)	0.26(0.15 – 0.36)	0.95(0.54 – 1.4)	0.77
”	”	8.7(8.0 – 9.5)	0.26(0.15 – 0.36)	0.9 (<i>fixed</i>)	0.76
GIS	2 – 4	8.7(7.7 – 9.9)	0.26(0.16 – 0.36)	1.02(0.65 – 1.4)	1.04
”	”	9.0(8.2 – 9.8)	0.26(0.15 – 0.36)	0.9 (<i>fixed</i>)	1.02
GIS	4 – 6	9.7(7.8 – 12.4)	0.31(0.13 – 0.50)	0.84(0.27 – 1.5)	0.89
”	”	9.5(8.3 – 11.3)	0.32(0.14 – 0.50)	0.9 (<i>fixed</i>)	0.87
GIS	0 – 6	9.0(8.3 – 9.7)	0.27(0.20 – 0.34)	1.04(0.79 – 1.3)	0.88
”	”	9.3(8.8 – 9.8)	0.27(0.20 – 0.34)	0.9 (<i>fixed</i>)	0.88
GIS + SIS	0 – 2	9.2(8.4 – 10.1)	0.25(0.17 – 0.34)	0.90(0.73 – 1.1)	0.94
”	”	9.2(8.6 – 9.8)	0.25(0.17 – 0.34)	0.9 (<i>fixed</i>)	0.94
GIS + SIS	2 – 4	9.2(8.3 – 10.2)	0.27(0.18 – 0.36)	1.06(0.81 – 1.3)	1.04
”	”	9.6(8.9 – 10.4)	0.27(0.18 – 0.36)	0.9 (<i>fixed</i>)	1.04

**Fig. 5.** Temperatures of the gas in A2390 determined for various radial zones by fits of a single-temperature model to the ASCA GIS (crosses) and ROSAT PSPC (diamonds) data. The ASCA points are for a fixed N_H at $9 \cdot 10^{21} \text{ cm}^{-2}$ (see Table 2). The errors are 90%-confidence limits.

respectively. The observed spectrum for each region is analyzed separately. The SIS data are limited to 4' radius. The data from the two GIS detectors, GIS2 and GIS3, and the two SIS detectors, SIS0 and SIS1, are respectively added for the analysis. The background data are obtained from the accumulated “blank fields” data from which the discrete sources are removed (Ikebe 1995) for the same radius regions of the detector f.o.v.

A single-temperature Raymond-Smith plasma model gives good fits to the data. The results for the GIS data are summarized in Table 2 in which the best-fit parameter values and the 90%-confidence limits (in parentheses) are listed. The results for the SIS data in the radius ranges 0' - 2' and 2' - 4' are fully consistent with those for the GIS data. The best-fit parameters determined from simul-

**Fig. 6.** ASCA GIS (●) and SIS (+) spectra inside the central 2'-radius of A2390. A single-temperature Raymond-Smith model is fit to both spectra simultaneously. The best-fit parameters are given in Table 2.

taneous fits to both the GIS and SIS data are also listed in Table 2. These results show that the plasma temperature is about 9 keV and the abundances is about 0.3 solar. The observed GIS and SIS spectra, not corrected for the instrument response, of the photons within 2' radius from the cluster center are shown in Fig. 6, together with the best-fit model to the combined data set. One can clearly see a peak around 5.5 keV which is due to the redshifted iron K_α lines.

The total flux within 6' radius is approximately $1.4 \cdot 10^{-11} \text{ erg s}^{-1} \text{ cm}^{-2}$ in the range 2 - 10 keV, and the bolometric flux is estimated to be $3 \cdot 10^{-11} \text{ erg s}^{-1} \text{ cm}^{-2}$. Thus

obtained bolometric luminosity of $8 \cdot 10^{45} h_{50}^{-2}$ erg s $^{-1}$ is in perfect agreement with the PSPC result.

4. Combined spectral analysis

The temperature as a function of radius obtained from the fits of a single-temperature model separately to the ASCA GIS and the ROSAT PSPC data is summarized in Fig. 5. As clearly seen in the figure, with use of a single-temperature model, the ROSAT PSPC spectrum shows a distinct cooling within 2' of the center. On the other hand, the ASCA GIS spectrum within 2' radius shows a much higher temperature than those obtained from the PSPC data. This apparent discrepancy suggests that the plasma is not of a single temperature but has a more complex temperature structure in the inner region. Suppose the plasma comprises components of different temperatures. The relative contributions of low-temperature components are larger in the ROSAT band (< 2 keV) than in the ASCA band (1 - 10 keV for the GIS). Hence, the ROSAT PSPC is sensitive to the contribution of low-temperature components. However, the ROSAT band does not give enough constraint on the high-temperature components. Most of the information on high-temperature components is contained in the ASCA band. For this reason the simultaneous use of both the ROSAT PSPC data and the ASCA GIS data provides maximum constraints on the multi-temperature plasma models.

We performed model fitting to the combined PSPC, GIS and SIS data for the inner 2' radius. A single set of model parameters is determined from the combined data, except for the normalization constants which are determined separately for the three instruments because of a possible systematic difference between them.

First, we employ a two-temperature model which assumes that the plasma within 2' of the center consists of a high-temperature component at T_H and a low-temperature component at T_L . The Raymond-Smith model is used for each component. The element abundances are assumed to be the same for both components. A good fit is obtained for a wide range of kT_L . As an example the fit of the model for $kT_L = 1.0$ keV to the data is shown in Fig. 7. The contribution of the low-temperature component in terms of the emission measure varies with kT_L , from about 4% for $kT_L = 0.5$ keV to about 15% for $kT_L = 2$ keV. The best-fit kT_H increases slightly with kT_L , from 9.3 keV for $kT_L = 0.5$ keV to 11.5 keV for $kT_L = 2$ keV. The best fit N_H is $(9 \pm 1) \cdot 10^{20}$ hydrogen atoms cm $^{-2}$. We note again that this value is somewhat larger than the galactic neutral hydrogen column at the cluster position of $6.7 \cdot 10^{20}$ cm $^{-2}$ (Dickey & Lockman 1990, Stark et al. 1992). (See Section 7.)

As shown below, it is not surprising that two-temperature models give a good fit to the combined ASCA and ROSAT PSPC spectra. To demonstrate that the above results are not produced by a forced fit, the

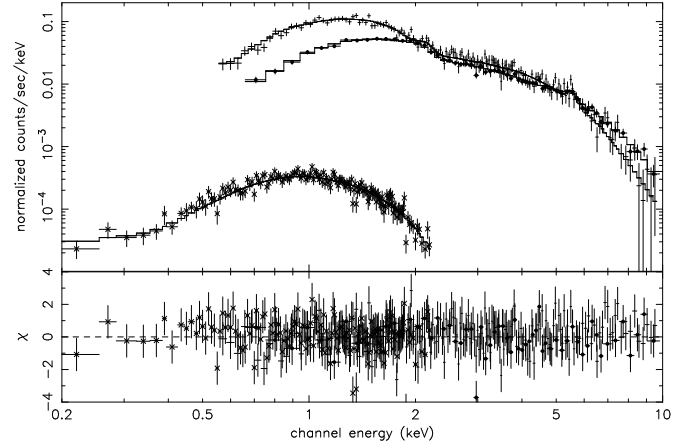


Fig. 7. Simultaneous fit to the GIS (●), SIS (+) and PSPC (*) spectra for the central 2'-radius region of A2390. A two-temperature Raymond-Smith model fits to the data with a reduced χ^2 -value of 0.97. The best-fit parameters are: $kT_H = 9.8$ keV, $kT_L = 1.0$ keV (fixed), $Z = 0.26Z_\odot$, $N_H = 8.8 \cdot 10^{20}$ cm $^{-2}$, $E_L/E_H = 0.05$, where E_H , E_L are the emission measures of the high- and low-temperature components.

two-temperature Raymond-Smith model is applied separately to the ASCA (GIS & SIS combined) data and the ROSAT PSPC data. Fig. 8 shows the acceptable ranges (90% confidence limit) of the temperature for the low-temperature component and its normalization factor (the emission measure relative to that of the high-temperature component), determined respectively for the ASCA and the ROSAT PSPC data. In fact, the acceptable regions for the two overlap each other over a wide range of kT_L . Therefore, for the parameter values within the overlap, the model can give an acceptable fit to the combined data set.

For a more realistic modelling, we employ a cooling flow model developed by Mushotzky and Szymkowiak (1988; see also Canizares et al. 1983; Johnstone et al. 1992), assuming a constant mass flow rate throughout the cooling flow and that the differential emission measure at a temperature T is proportional to the cooling time (hence inversely proportional to the bolometric luminosity at T). This model includes five parameters: mass accretion rate \dot{M} , a parameter which describes the distribution of emission measure versus temperature, s , abundances of the elements, the initial plasma temperature, T_H , the lowest temperature of the cooling flow relevant for the X-ray observation, T_L . We require pressure equilibrium in the cooling flow, which corresponds to the case where $s = 0$. A contribution of emission from non-cooling high-temperature (at T_H) plasma is also included, considering

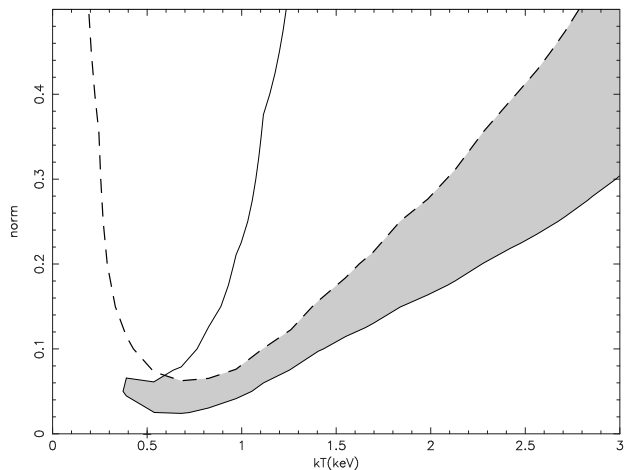


Fig. 8. The 90%-confidence contours for the two-temperature Raymond-Smith model determined separately for the combined GIS and SIS spectra (dashed curve) and for the ROSAT PSPC spectrum (solid curve), both within the central $2'$ -radius of the cluster. The parameters varied are the temperature of the low-temperature component and the normalization factor (the emission measure relative to that of the high-temperature component). For the ASCA data N_H was fixed to 10^{21} cm^{-2} . For the PSPC data kT_H and the abundances were fixed to 9.5 keV and $0.3 Z_\odot$, respectively. The acceptable domains are inside the solid curve extending to upper right for the PSPC data and below the dashed curve for the ASCA data, overlapping in the shaded region.

the case in which only a part of the plasma within the projected radius of $2'$ is involved in the cooling flow. In fact, no acceptable fit can be obtained without inclusion of a non-cooling component. In the fitting, T_L was fixed at 0.5 keV, since the result is practically insensitive to the T_L value chosen in the range 0.1 - 1 keV. A good fit is obtained with this model, as shown in Fig. 9. The best-fit result shows that $kT_H \cong 12.1$ keV and $\dot{M} \cong 700 M_\odot \text{ yr}^{-1}$ with the 90%-confidence range $400\text{--}850 M_\odot \text{ yr}^{-1}$ and that still approximately 80% of the observed flux within $2'$ radius comes from the non-cooling high-temperature plasma.

The $2'$ -radius data alone do not have a statistical accuracy to constrain kT_H well enough, accepting a fairly wide range up to 18.5 keV (90% confidence limit). A tighter limit on kT_H can be obtained by using the GIS data within the $6'$ -radius circle that have the best statistical accuracy. We assume isothermality of the hot component within this radius and include the central cooling component with \dot{M} determined above. Employing the telescope response for the brightness profile determined from the ROSAT data, we obtain the 90% confidence limits of kT_H to be 9.5–12.6 keV (with the best-fit of 11.1 keV) for the acceptable range of \dot{M} . Similar results are also obtained from simultaneous

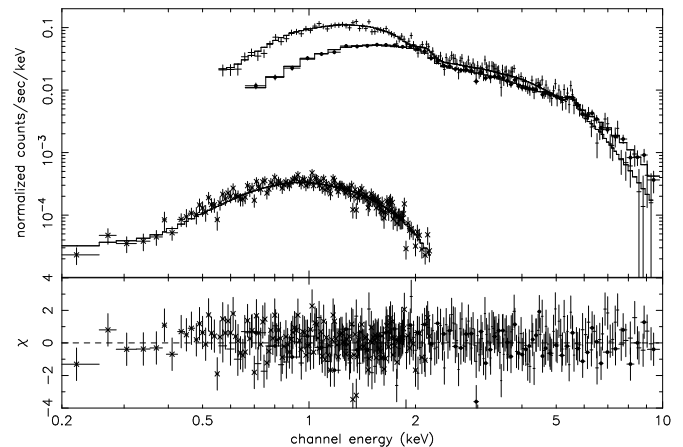


Fig. 9. Simultaneous fit of a cooling flow model (including a contribution of non-cooling hot component) to the GIS (\bullet), SIS (+) and PSPC ($*$) spectra for the central $2'$ -radius circle of A2390. The model gives a good fit to the combined data (reduced χ^2 of 0.97) with the following best-fit parameters: $kT_H = 12.1$ keV, $\dot{M} \sim 700 M_\odot \text{ yr}^{-1}$, $Z = 0.3 Z_\odot$, $N_H = 8.7 \cdot 10^{20} \text{ cm}^{-2}$.

fit of a model comprising an isothermal hot plasma and a cooling flow to the $2'$ -radius PSPC and SIS data and $6'$ -radius GIS data, thus confirming that the temperature of the hot component is not much higher than 12 keV.

5. Mass determination

From the surface brightness profile of the cluster obtained from the ROSAT PSPC and HRI observation we can determine the gas distribution in the cluster. We use the analytical description of the surface brightness of the β -model to deproject the surface brightness. Since the plasma emissivity in the ROSAT band in the temperature range of interest (3 to 12 keV) depends only insignificantly on the temperature we directly derive the emission measure distribution and the gas density distribution from these observations. The resulting gas mass profile is shown in Fig. 10.

Under the assumption that the intracluster medium of A2390 is approximately in hydrostatic equilibrium and that the cluster can be approximated as being spherically symmetric we can derive the profile of the gravitating cluster mass from the derived gas density and temperature profiles by means of the hydrostatic equation which can be written in the following form:

$$M(r) = -\frac{kT_g(r) r}{m_h \mu G} \left(\frac{d \log T_g(r)}{d \log r} + \frac{d \log \rho(r)}{d \log r} \right) \quad (2)$$

It has been shown by N-body/hydrodynamical simulations of cluster formation by Schindler (1996) and Evrard et al. (1996) that the assumption of hydrostatic equilibrium does in general not lead to a large error ($\leq 15-20\%$) in the mass determination, if cases of strong deviation e.g. such as found in cluster mergers are avoided. For A2390 which seems to be a well relaxed cooling flow cluster, large deviations are not to be expected. It was also demonstrated c.f. in Neumann and Böhringer (1996, see also White et al. 1994, Buote & Canizares, 1996) that ellipticities of the order observed for A2390 can be azimuthally averaged into an azimuthally symmetric model without causing an error larger than a few percent in the derived mass. Thus, the main source of error in this analysis is still the uncertainty in the temperature profile of the cluster, and the above applied simplifications are well justified.

To explore the range of possible temperature profiles we have calculated a series of polytropic models, where the nominal temperature was fixed at the core radius. The models include the following parameter combinations which well cover the range allowed by the temperature measurements for the models including the cooling flows: $kT = 9.5, 11,$ and 12.5 keV with $\gamma = 0.9, 1.0, 1.1,$ respectively for all nominal temperatures. Fig. 10 shows the resulting profiles for the maximal and minimal mass as a function of the radius. This range of models allows for some temperature variation such that for example at a radius of 2 arcmin ($0.65 h_{50}^{-1}$ Mpc) temperatures in the range of 8.8 to 13.5 keV are accepted. The dotted line gives the mass profile for an isothermal model with a gas temperature of 11 keV.

As mentioned above, the temperature of the hot component in the inner 1 - 2 arcmin region is not well constrained at the high-temperature side if a cooling flow model is considered. In the mass models given in Fig. 10, we considered the temperature of the hot component at the core radius up to 12.5 keV. This value is about the upper limit of the temperature determined with the ROSAT PSPC for the next outer ring (1' to 2') which is hardly affected by the cooling flow region. In addition, the ASCA GIS data give an upper limit of 12.6 keV within 6' radius. In fact, due to the broad PSF of the ASCA telescopes, about 70% of the photons inside the 6'-radius circle of the observed GIS image come from the inner 2' of the cluster center (Ikebe 1995). Thus, the temperature of the hot component within 2' cannot be much higher than 12.5 keV.

At the limiting radius of the X-ray emission, at $2.5 h_{50}^{-1}$ Mpc, we find a cluster mass of $1.9(1.1 - 3.1) \cdot 10^{15} M_{\odot}$, and extrapolated to 3 Mpc the mass increases to $2.3(1.3 - 3.8) \cdot 10^{15} M_{\odot}$. For comparison, this cluster has a similar mass to the Coma Cluster whose mass is about $1.1 - 2.8 \cdot 10^{15} M_{\odot}$ (Briel et al. 1992, see also Böhringer 1994 for a more comprehensive set of model calculations).

For the ratio of the X-ray luminous mass to the total mass of A2390 (which sets an interesting lower limit to the

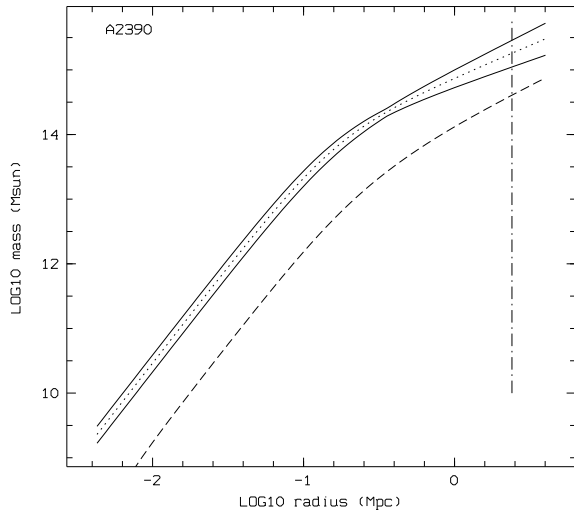


Fig. 10. Radial mass profile of A2390 determined from the ASCA and ROSAT X-ray observations. The dashed line gives the gas mass profile determined from the best-fit β -model. The solid lines give the upper and lower limits of the gravitational mass profiles for the cluster as determined from a family of polytropic models over the temperature range allowed by the X-ray spectral analysis. The dotted line in the mass profile corresponds to the isothermal case for $kT = 11$ keV. The vertical dashed line indicates the radius out to which X-ray emission is significantly observed, hence any reliable statement can be made.

baryon mass fraction of the cluster) we find for the outer X-ray radius ($2.5 h_{50}^{-1}$ Mpc) a value 23 (14 - 40) %. There is a trend of an increasing gas mass fraction with radius which is due to the fact that the surface brightness slope parameter β is smaller than one. We find the following gas to total mass ratios for different radii: 9 (7-11) % at $175 h_{50}^{-1}$ Mpc (the arc radius), 18 (13 - 25) % at $1 h_{50}^{-1}$ Mpc, and 24 (14 - 40) % at $3 h_{50}^{-1}$ Mpc. Note that this indicates the importance of information on the X-ray emission out to large radii as obtained by the PSPC observations. An extrapolation of the slope of the surface brightness profile found in the HRI observation would lead to quite different results: a little smaller gravitational mass due to the shallower gas density gradient but a much larger gas mass, thus leading to an erroneous gas mass fraction at large radii for this cluster.

6. Comparison to gravitational lensing results

The mass determined by means of the X-ray observations can now be compared to the mass inferred from the gravitational lensing result. This is of great interest because both methods are based on completely different physical principles and are subject to very different effects. For example, the gravitational lensing method does not require the condition of virial or hydrostatic equilibrium of the

cluster, while it is more sensitive to the projection effects of masses in the line of sight. Therefore, the comparison of the results obtained from both methods provides an important confirmation that the assumptions made in the derivation of the cluster mass are justified.

For the comparison we have to calculate the projected cluster mass profile onto the observer plane. We calculate it, cutting the 3-dimensional mass profile at an outer radius of $3 h_{50}^{-1}$ Mpc, which is within the uncertainties equal to the virial radius of the cluster. The results are shown in Fig. 11 and compared to the lensing results from strong lensing by Pierre et al. (1996) and for weak lensing by Squires et al. (1996). The agreement is excellent. Since the mass models shown in Fig. 10 and 11 are calculated from the non-deconvolved PSPC data, we examine the effect of the limited resolution by calculating a mass model based on the inner HRI surface brightness profile with an estimated deconvolved core radius of 6 arcsec. The resulting mass profile, also shown in Fig. 11, is higher and less steep near the center, but does not affect the result at and outside the radius of the arc. Similarly, an exact treatment of the multi-temperature structure of the cooling flow region would somewhat modify the mass profile. However, since the cooling flow also lies inside the arc radius, the mass profile will not be affected by the cooling flow at the radii relevant for the comparison to the lensing results. Therefore, the good agreement is independent of the uncertainties in the mass profile due to the limited resolution of the observation and of the cooling flow structure. One should note, however, that the weak lensing mass result tends to be biased towards a low value, as carefully described in Squires et al. (1996), due to the fact that not all the cluster mass is covered by the optical observation on which the lensing analysis is based. Yet, this should lead to a relatively small correction, since the mass profile is traced by the lensing result already out to a radius of about $1 h_{50}^{-1}$ Mpc.

7. Cooling flow

The first argument for the existence of a cooling flow in A2390 comes from the calculated short cooling time of less than about $3 \cdot 10^9$ y for the central region. Adopting a cluster age of 10^{10} y, we find a cooling radius, the radius at which the cooling time equals the cluster age, of $\sim 160 h_{50}^{-1}$ kpc. We estimate the mass flow rate of the cooling flow in the standard way, assuming a steady-state, comoving, non-heat-exchanging cooling flow model, in a simple and more explicit way. In the simple model we set the integral radiation loss inside a spherical volume of the cluster equal to the enthalpy influx

$$\int_0^R n_e n_p \Lambda(T(r)) dV(r) = \frac{5kT}{2\mu m_p} \dot{M}(R) \quad (3)$$

where $\Lambda(T)$ is the cooling function, and μm_p is the mean particle mass. One can also calculate the mass flow

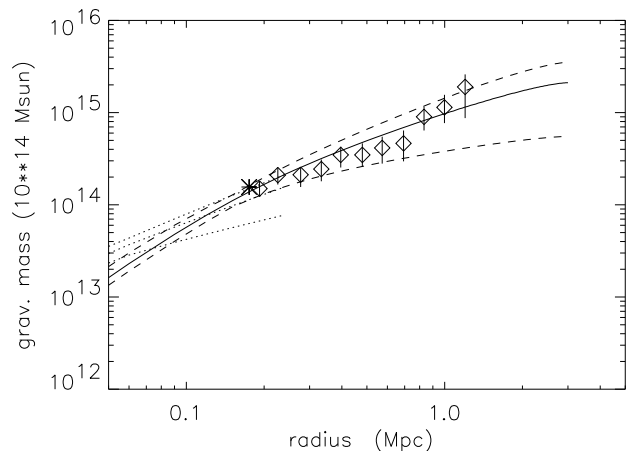


Fig. 11. Radial mass profile of A2390. The mass model is the same as shown in Fig. 10, but projected onto the observer plane with a cut-off of three-dimensional radius at $3 h_{50}^{-1}$ Mpc. The three dotted lines show the corresponding model calculations when the surface brightness fit to the HRI data is used for the inner region. The asterisk is the result from the strong lensing model by Pierre et al. (1996), and the diamonds show the results of the weak lensing analysis by Squires et al. (1996).

rate by considering the energy balance in a differential way also allowing for the energy gain of the gas flowing down the gravitational potential of the cluster:

$$n_e n_p \Lambda(T) = \frac{\dot{M}}{4\pi r^2} \left(\frac{5k}{2\mu m_p} \frac{dT}{dr} + \frac{d\phi}{dr} \right) + \frac{d\dot{M}}{dr} \frac{1}{4\pi r^2} \frac{5kT}{2\mu m_p} \quad (4)$$

where $\phi(r)$ is the gravitational potential of the cluster. Both approaches lead to very similar results. The values for the mass flow from the second formula are lower by only about 10-20% because of the gravitational energy input. The estimated mass flow rates at the cooling radius are in the range 550 to $700 M_{\odot} y^{-1}$. These results are absolutely consistent with the results of Pierre et al. (1996). They get larger numbers for the cooling radius and the mass flow rate for an assumed cluster age of $1.4 \cdot 10^{10}$ years. The difference between their results and ours is only due to different ages assumed.

As described in Section 4, a mass flow rate around $700 M_{\odot} y^{-1}$ is obtained from the spectral fitting of the multi-temperature cooling flow model to the combined ASCA GIS and ROSAT PSPC data. This is in very good agreement with the result from the radial surface brightness profile of the X-ray image. Thus, the same results have been found in two completely independent ways.

The cooling flow rate inferred from the imaging data implies in the case of a steady state a certain residence time of the cooling matter per intermediate temperature interval. This defines the emission measure distribution

$E(T)$ as a function of temperature, expressed by the equation:

$$E(T)\Lambda(T)dT = \frac{5k}{2\mu m_p} \frac{\dot{M}}{\Lambda(T)} dT \quad (5)$$

The normalization of $E(T)$ is the cooling flow parameter determined in the spectral analysis. Therefore, the fact that the two cooling flow rates obtained from the spectral and the imaging data agree with each other implies that all the observed properties are consistent with the standard model of the cooling flow structure. In this case, the cluster must have had a long time ($\sim 10^{10}$ y) to develop this cooling flow. Otherwise, the steady-state cooling radius should be smaller for shorter times, resulting in a smaller cooling flow rate inconsistent with the spectral result. Similar consistency for such a cooling flow analysis was found in the study of crystal spectrometer data from the EINSTEIN Observatory (Canizares et al. 1983) and recently for a similar combined ASCA-ROSAT study of some clusters by Allen et al. (1996, see also Allen 1997).

As noted in Section 2, the absorbing hydrogen column density inferred from the spectral data (independently from ROSAT and ASCA) indicate a higher value than measured in 21 cm for the intervening interstellar matter of our galaxy. To check if this could be absorption caused by cold material in the cooling flow of the clusters - such as observed in other cluster cooling flows (e.g. White et al. 1991, Allen et al. 1997, Allen 1997) - we studied the radial distribution of the excess absorption in detail in the PSPC observation. For the radial zones, 0 - 2 arcmin, 2 - 4 arcmin, and 4 - 6 arcmin we find values for n_H of 0.93 (0.84-1.1), 0.81 (0.6-1.2), and an unconstrained value in the range (0.3 - 2.0) in units of 10^{21} cm $^{-2}$, respectively. The range in brackets indicates 2σ limits. The N_H -value in the second ring not influenced by the cooling flow is still high, but not inconsistent within 2σ with the galactic value of $6.7 \cdot 10^{20}$ cm $^{-2}$ from the 21 cm data (Dickey & Lockman 1990; Stark et al. 1992). This result is consistent with an excess absorption in the cooling flow region, though not conclusive. We note that the absorption values in the Stark et al. (1992) map were only derived for a grid spacing of two degrees. Therefore, it is still possible that the excess absorption found in the X-ray observation of A2390 is due to a variation in the galactic hydrogen column. An inspection of the IRAS 100μ maps gives no indication of an enhanced interstellar column density in our galaxy in the line of sight of A2390 with the best estimate for N_H of about $4.6 \cdot 10^{20}$ cm $^{-2}$.

8. Conclusions

The present study of A2390 with combined use of the ROSAT PSPC and ASCA GIS data yields important new results. The two most striking results of the current study are (1) good consistency between the cooling flow rates

derived independently from the spectral and imaging analyses, and (2) excellent agreement between the total mass values determined from the X-ray data and the gravitational lensing. As outlined in the introduction, the cluster shows all the apparent features of a well relaxed cluster: elliptical symmetry, strong central concentration (and a cD galaxy which may be the result of this), a cooling flow, and a large intracluster light halo around the central galaxy. A long cooling time ($\sim 10^{10}$ y) implied from the cooling flow rate may be taken as a reinforcement of the picture that the cluster was left quite undisturbed for a long time.

In the morphological analysis of the HRI image of A2390 Pierre et al. (1996) found some indication of substructure in the cluster. They interpreted the substructural feature as a trace of substructure in the cluster potential, and such an excess potential is actually needed in the gravitational lensing model producing the observed gravitational arc. The subclump has an X-ray luminosity of only about 1/60 of that of the whole cluster and therefore its mass is less than about 1/15 of that of the cluster as concluded by Pierre et al. (1996). Such a small infalling mass component will not cause a significant disturbance on the equilibrium configuration of the cluster, and also may not influence the evolution of the cooling flow seriously. Therefore, the presence of this small substructure is not in contradiction to our finding that the cluster is generally well settled.

The large measured iron abundance of ~ 0.3 of the solar value is in line with other observed results for very rich nearby clusters and some distant clusters. We should note, however, that lower abundances have been found in some rich distant clusters like CL0016+16 (Furuzawa et al. 1997) and A851 (Mushotzky & Loewenstein, 1997, Schindler et al. 1998).

Earlier studies have pointed out cases of striking differences between the lensing mass and X-ray determined mass (e.g. Miralda-Escudé & Babul 1995). The reason for an excellent agreement between the two in A2390 is most probably found in that this cluster is fairly relaxed, as compared to other clusters studied by weak lensing technique and X-ray observations. For example, A2218 and A2163 show signs of recent merging (Squires et al. 1996b, 1997). The detailed study of A2218 shows a tendency that the lensing mass is higher than the X-ray mass, while in A2163 the two mass values are well consistent with each other. PKS0745 which also shows a strong cooling flow and a gravitational arc (Allen et al. 1996) may be in a similar situation to A2390, and consistency between the lensing mass and X-ray mass could be found in this system, too. Allen et al. (1996) have already stressed that the agreement of the mass determination in PKS0745 is most probably the result of the cluster being well relaxed (see also recent work in Allen 1997).

Acknowledgements. H.B. thanks for support by the Verbundforschung under the grant No. 50 OR 93065. Y.T. is grateful

for the hospitality of Max-Planck-Institut für Extraterrestrische Physik where he conducted part of this work.

References

- Abell, G.O., 1958, *ApJS*, 3, 211
- Abell, G.O., Corwin, H.G. & Olowin, R.P., 1989, *ApJS*, 70, 1
- Allen, S.W., Fabian, A.C., Kneib, J.P., 1996, *MNRAS*, 279, 615
- Allen, S.W. & Fabian, A.C., 1997, *MNRAS*, 286, 583
- Allen, S.W., 1997, preprint at *astro-ph-9710217*
- Arnaud, M., Rothenflug, R., Böhringer, H., Neumann, D.M., Yamashita, K., 1996, *A&A* (in preparation)
- Bartelmann, M. & Steinmetz, M., 1996, *MNRAS*, 283, 431
- Böhringer, H., 1994, in “Cosmological Aspects of X-ray Clusters of Galaxies”, W.C. Seitter (ed.), NATO ASI Series C Vo. 441, Kluwer Academic Publ., p. 123
- Briel, U.G., Henry, J.P., Böhringer, H., 1991, *A&A*, 259, L31
- Buote, D.A. & Canizares, C.R., 1996, *ApJ*, 457, 565
- Canizares, C.R., Stewart, G.C., Fabian, A.C., 1993, *ApJ*, 272, 449
- Cavaliere, A. & Fusco-Femiano, R., 1976, *A&A*, 49, 137
- Dickey, J.M. & Lockman, F.J., 1990, *ARAA*, 28, 215
- Ebeling, H., Voges, W., Böhringer, H., Edge, A.C., Huchra, J.P., Briel, U.G., 1996, *MNRAS*, 281, 799
- Edge, A.C. & Stewart, G.C., *MNRAS*, 252, 428
- Evrard, A.E., Metzler, C.A., Navarro, J.N., 1995, *ApJ*, 469, 494
- Furuzawa, A., Tawara, Y., Kunieda, H. et al. 1997, to appear in *ApJ*
- Ikebe, Y., 1995, PhD. Thesis, Tokyo University
- Johnstone, R.M., Fabian, A.C., Edge, A.C., & Thomas, P.A., 1992, *MNRAS*, 255, 431
- Jones, C. & Forman, W., 1984, *ApJ*, 276, 38
- Kassiola, A., Kovner, I. & Blandford, R.D., 1992, *ApJ*, 396, 10
- Le Borgne, J.F., Mathez, G., Mellier, Y., Pello, R., Sanahuja, B., Soucail, G., 1991, *A&AS*, 88, 133
- McMillian, S.L.W., Kowalski, M.P., Ulmer, M.P., 1989, *ApJS*, 70, 723
- Miralda-Escudé, J. & Babul, A., 1995, *ApJ*, 449, 18
- Mushotzky, R.F. & Szymkowiak, A.E., 1988, in “Cooling flows in Clusters of Galaxies”, A.C. Fabian (ed.), Kluwer Academic Publ., p. 47
- Mushotzky, R.F. & Loewenstein, M., 1997, *ApJ*, 481, L63
- Narashima, D. & Chitre, S.M., 1993, *J. Astr. Astrophys.*, 14, 121
- Neumann, D.M. & Böhringer, H., 1997, *MNRAS*, 289, 123
- Pelló, R., LeBorgne, J.F., Soucail, G., Mellier, Y., Sanahuja, B., 1991, *ApJ*, 366, 405
- Pierre, M., Le Borgne, J.F., Soucail, G., & Kneib, J.P., 1996, *A&A*, 311, 413
- Schindler, S., 1996, *A&A*, 305, 756
- Schindler, S., Belloni, P., Ikebe, Y., Hattori, M., Wambsganss, J., Tanaka, Y., 1998, *A&A*, submitted
- Squires, G., Kaiser, N., Fahlman, G., Babul, A., & Woods, D., 1996a, *ApJ*, 469, 73
- Squires, G., Kaiser, N., Fahlman, G., Woods, D., Babul, A., Neumann, D.M., Böhringer, H., 1996b, *ApJ*, 461, 572
- Squires, G., Neumann, D.M., Kaiser, N., Arnaud, M., Babul, A., Böhringer, H., Fahlman, G., Woods, D., 1997, *ApJ*, 482, 648
- Stark, A.A., Gammie, C.F., Wilson, R.W., Bally, J., Linke, R.A., Heiles, C., Hurwitz, M., 1992, *ApJS*, 79, 77
- Ulmer, M.P., Kowalski, M.P., Cruddace, R.G., 1986, *ApJ*, 303, 162
- Vílchez-Gómez, R., Pelló, R., Sanahuja, B., 1994, *A&A*, 283, 37
- White, D.A., Fabian, A.C., Johnstone, R.M., Mushotzky, R.F., Arnaud, K.A., 1991, *MNRAS*, 252, 72
- White, D.A., Fabian, A.C., Allen, S.W., Edge, A.C., Crawford, C.S., Johnstone, R.M., Stewart, G.C., Voges, W., 1994, *MNRAS*, 269, 589
- Yee, H.K.C., Ellingson, R.G., 1996a, *ApJS*, 102, 269
- Yee, H.K.C., Ellingson, E., Abraham, R.G., Gravel, P., Carlberg, R.G., Smecker-Hane, T.A., Schade, D., Rigler, M., 1996b, *ApJ*, 102, 289